ACS APPLIED MATERIALS & INTERFACES

Research Article

www.acsami.org

Dispersed Cu_2O Octahedrons on h-BN Nanosheets for *p*-Nitrophenol Reduction

Caijin Huang, Weiqing Ye, Qiuwen Liu, and Xiaoqing Qiu*

Research Institute of Photocatalysis, State Key Laboratory of Photocatalysis on Energy and Environment, College of Chemistry, Fuzhou University, 523 Gongye Road, Fuzhou 350002, China

Supporting Information

ABSTRACT: We demonstrate here that two-dimensional boron nitride (h-BN) nanosheets can be employed as a robust supporting substrate to incorporate function metal oxides. The Cu_2O@h-BN composites are thus obtained by dispersing Cu_2O octahedrons on the surfaces of h-BN nanosheets. The −OH and −NH groups on the surfaces of h-BN nanosheets are found to be beneficial for anchoring Cu_2O octahedrons. Moreover, the Cu_2O@h-BN composites exhibit superior activity for the reduction of *p*-nitrophenol to pure Cu_2O crystals and h-BN nanosheets. The h-BN component in the composites plays a critical role in the formation and adsorbing of the *p*-nitrophenolate ions, and, at the same time, Cu_2O components react with brohydride ions and transfer a surface hydrogen species and electrons, resulting in the reduction of *p*-nitrophenol into *p*-aminophenol. Our results provide a new approach for the rational design and development of metal oxides composites and open the way to a range of important applications of h-BN-based materials.

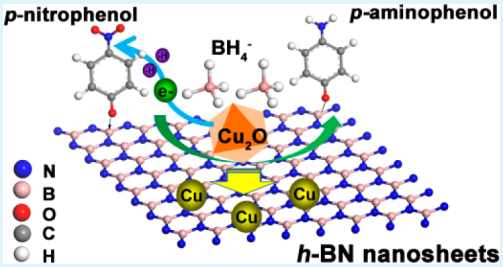

KEYWORDS: *Cu_2O, h-BN, supporting substrates, composites, p-nitrophenol reduction*

INTRODUCTION

Nowadays, metal oxides are undoubtedly one of the most widely investigated functional materials due to their variety of structures and properties, and their technological applications.[1−3] However, the strong interactions of the oxides particles, especially for their nanostructured counterparts, cause them to clump and aggregate,[4] thereby deteriorating the relevant properties. Accordingly, dispersing metal oxide particles on various supporting substrates is regarded as a very promising approach for preventing the interparticle aggregation.[5−11] For instance, Sarkar et al. summarized the polymer-supported metals and metal oxides and concluded that the many shortcomings can be overcome by appropriately dispersing the functional particles into polymeric/biopolymeric host materials.[7] Reddy and Ramaprabhu demonstrated that multiwalled carbon nanotubes served as a good supporter to disperse metal oxides for the supercapacitor application.[6] Recently, Tour and his co-workers reported that the sintering and aggregation of Fe_2O_3 nanoparticles can be effectively inhibited even during the high temperature treatment (800 °C) by dispersing the Fe_2O_3 nanoparticles on graphene sheets.[5] Among these various substrates, two-dimensional supporters are appealing candidates because they provide a platform for attaching the particles and endowing the "naked" particle surface with high active sites.[12] Two-dimensional hexagonal boron nitride (h-BN) nanosheet, a structural analogue of graphene, is a robust substrate due to its advantages of atomically smooth surfaces, transparency, nontoxicity, and structural stability.[13−15] Many elaboration works have been devoted to the properties and potential application of h-BN nanosheet such as electrical resistance, thermal conductivity, catalytic activity, and optoelectronic properties.[16−22] Surprisingly, as compared to the significant progress achieved in the graphene-based materials,[23−25] the h-BN-supported composites have been lingering far behind. Along with the recent progress in exfoliation and stabilization of h-BN nanosheets,[26,27] various efforts have been made to incorporate the h-BN nanosheets with other materials, primarily focusing on noble metal nanoparticles.[28,29] From the viewpoint of both basic science and technological applications, it is therefore highly desirable to develop a simple and effective method for dispersing the functional metal oxides on the h-BN nanosheets. This move would not only shed light on our mechanistic understanding of chemical formation of the composites in general, but also allow us to better integrate these merits of h-BN and metal oxides in advanced device design and practical applications.

In particular, cuprous oxide (Cu_2O) is a well-known functional material and widely investigated for its potential application in catalysis,[30] biocides,[31] gas sensors,[32] solar energy photovoltaics,[33] and lithium-ion batteries.[34,35] It is reported that the Cu_xO clusters with Cu(I) specially dispersed on the surfaces of TiO_2 endow the resulting composites with the antimicrobial properties and the efficient visible-light photooxidation of volatile organic compounds.[36] In addition, it has been also demonstrated that enhancement of photocatalytic activity and stability can be achieved by dispersing Cu_2O

Received: June 13, 2014
Accepted: July 21, 2014
Published: July 21, 2014

particles on the graphene oxide.[37−40] Recently, our group has successfully exfoliated the bulk h-BN into few-layer nanosheets based on the matching of the surface energies of h-BN and the surface tension of the solvent, which can be used as good carriers to disperse noble metal nanoparticles, such as Ag, Au, and Pt.[41] Subsequently, the h-BN nanosheets are highly expected to support the functional oxides particles, which opens the way to a range of important applications of h-BN-based materials. Herein, we attempted to disperse the Cu_2O octahedral on the h-BN nanosheets, and investigated the feasibility of using the obtained Cu_2O@h-BN composites as catalysts for the reduction of *p*-nitrophenol to *p*-aminophenol. Generally, *p*-nitrophenol is one of the most common organic pollutants in the water that originates from agricultural and industrial sources, while *p*-aminophenol is an important intermediate for pharmaceuticals. Thus, the conversion of nitro group to amino group has great industrial relevance. It is found that the Cu_2O@h-BN composites show promising efficiency in the reduction of *p*-nitrophenol to *p*-aminophenol.

EXPERIMENTAL SECTION

Sample Preparation. The synthesis of the h-BN powder was reported in our previous work.[41] In a typical procedure, boric acid and urea with a molar ratio of 1:24 were fully dissolved in 40 mL of ultrapure water, which was dried at 65 °C to form a white precursor. The resulting precursor was subjected to heat treatment in a tube furnace up to 900 °C for 5 h in a N_2 atmosphere. The pyrolytic product was sufficiently washed with dilute hydrochloric acid and absolute ethanol, dried in air at ambient temperature, and ground into powder using an agate mortar.

To prepare Cu_2O@h-BN composites, 20 mg of the as-obtained h-BN powder was first dispersed into 100 mL of ultrapure water by ultrasonication for 30 min to give a white suspension. One milliliter of $CuCl_2$ aqueous solution (0.05 M) was then added into 9 mL of the above h-BN suspension under magnetic stirring for 20 min. Subsequently, 1 mL of NaOH aqueous solution (0.5 M) was added into the mixture with stirring. After further stirring for 30 min, 1 mL of 0.1 M glucose solution was added into the above suspension. The reaction was then heated at 50 °C until the formation of a brick red dispersion. The products were washed several times with water, and dried at 70 °C in an oven. For comparison, pure Cu_2O was also prepared by the same procedure without the addition of h-BN suspension.

Sample Characterization. The phase structural charateristics of the samples were investigated by powder X-ray diffraction (XRD) patterns at room temperature on a PANalytical X'Pert spectrometer using Co Kα radiation (λ = 0.1788 nm), and the data were changed to Cu Kα data. The Fourier transform infrared spectroscopy (FT-IR) analyses were performed on a nicolet 670 FT-IR spectrometer, using a KBr pellet technique. Raman spectroscopy was carried out on a Renishaw inVia Raman Microphrobe at 532 nm laser excitation. The X-ray photoelectron spectroscopy (XPS) was collected on a SHIMADZU (Amicus), using Mg Kα X-ray as an excitation source (1486.8 eV). The morphologies and microstructures of the samples were investigated by field emission scanning electron microscopy (FESEM) on a Hitachi New GenerationSU8010 apparatus and transition electron microscopy (TEM) on a TECNAI F30 instrument under an acceleration voltage of 200 kV.

Catalytic Activity Test. Typically, 5 mL of *p*-nitrophenol aqueous solution (200 ppm) and 5 mL of freshly prepared aqueous $NaBH_4$ (0.1 M) were successively added into 70 mL of deionized water in a beaker, stirring constantly for all of the experiments. Next, 10 mg of catalysts was added into the mixture. The concentration of *p*-nitrophenol in the supernatant was monitored by the UV−visible absorption spectra recorded on a Cary-50 UV−visible spectrometer (Cary 50, VARIAN). For recycling experiment, the catalysts were collected by membrane filtration after the reaction, dried at 70 °C, and then reused.

RESULTS AND DISCUSSION

Figure 1a gives the XRD patterns of the as-obtained BN powder. As can be seen, the *d*-spacings of the diffraction peaks

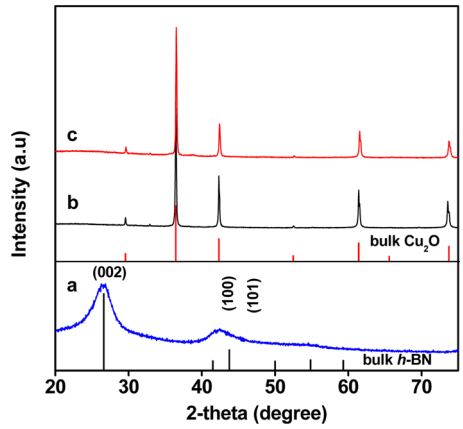

Figure 1. XRD patterns of the samples: (a) h-BN, (b) Cu_2O, (c) Cu_2O@h-BN composites.

of our synthesized samples match well with the standard data for bulk h-BN with a layered structure (JCPDS card no. 85-1068), except for the apparent peak broadening due to its low crystallinity. Moreover, as shown in Figure 1b, the diffraction peaks of Cu_2O can be easily indexed to a pure cubic phase of cuprous oxide (JCPDS card no. 77-0199). The intense and sharp peaks indicate the high crystallinity of Cu_2O sample. After incorporation of Cu_2O and h-BN, it could be clearly found the close resemblance of the XRD patterns of the composites to that of pure Cu_2O (Figure 1c). However, the typical diffraction peaks corresponding to the h-BN appear to be negligible in the composites, due to its relatively weak diffraction intensity and good exfoliation of the h-BN nanosheets in the composite during the synthesis procedure with the assistance of ultrasonication, which will be described later.

Considering the detection limit of XRD measurement, the infrared spectra of samples were investigated to obtain the further chemical component information. Figure 2a gives the FTIR spectra of h-BN, Cu_2O, and Cu_2O@h-BN composites. The FTIR spectrum of h-BN alone contains two characteristic absorption bands at 1380 and 780 cm^{-1}, which correspond to the in-plane B−N stretching mode (E_{1u}) and the plane B−N−B bending mode (A_{2u}), respectively.[14,42] It is also noted that the broad absorption bands centered at 3400 and 3185 cm^{-1} were observed, which can be assigned to the surface residual bonded OH and NH groups,[43] respectively. Pure Cu_2O sample shows a diagnostic intense Cu−O vibration band located at 630 cm^{-1}.[44,45] In the case of Cu_2O@h-BN composites, the FTIR spectrum displays the evident absorption peaks in the range of 1700−700 cm^{-1}, similar to the h-BN, besides the presence of the Cu−O vibration band of Cu_2O. Additionally, as compared to the spectrum of h-BN, the intensity of the absorption peaks corresponding to surface −OH and −NH groups has a significant decrease in the Cu_2O@h-BN composites, implying that the surface −OH and −NH groups can serve as the active sites to attach Cu_2O particles on the h-BN nanosheets. Moreover, Raman spectroscopy was next used to get the microstructure details due to its high sensitivity and non-destructive nature. As shown in Figure 2b, it is clear that h-BN

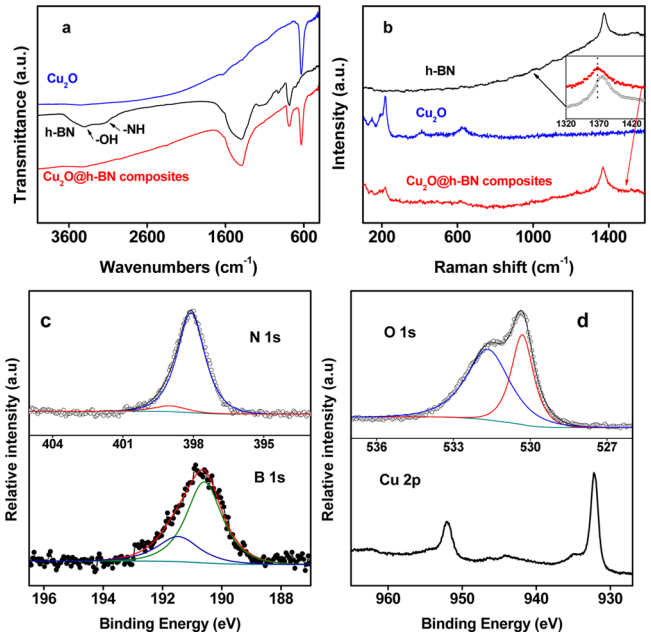

Figure 2. (a) FTIR spectra and (b) Raman spectra of the as-obtained samples. Inset: The enlarged spectra. (c) N 1s and B 1s core-level spectra of the Cu_2O@h-BN composites, (d) O 1s and Cu 2p core-level spectra of the Cu_2O@h-BN composites.

powder sample shows one prominent characteristic peak at about 1375 cm^{-1}, which can be assigned to the high-frequency E_{2g} vibrating mode of h-BN.[42] In contrast to bulk h-BN,[46] this E_{2g} mode is broadened and shifted to higher wavenumber, suggesting that our h-BN sample was poorly crystallized,[47] which might be beneficial for the exfoliation under the ultrasonication. In addition, the Raman spectrum of Cu_2O shows the diagnostic phonon frequencies of the cubic structure with a space group of *Pn*3*m*. The strong peak at 220 cm^{-1} corresponds to the second-order Raman active mode of the Cu_2O crystals, while the shoulder peak at 151 cm^{-1} can be ascribed to Raman scattering from phonons of symmetry.[48,49] Furthermore, two relatively weak vibration dynamic peaks at 412 and 615 cm^{-1} are attributed to the Γ_{1-5} Raman mode of Cu_2O.[50] Obviously, the characteristic Raman spectral signatures of both h-BN and Cu_2O are presented in the Cu_2O@h-BN composites, demonstrating the efficient incorporation of Cu_2O and h-BN. Very interestingly, the E_{2g} mode of h-BN component of the composites is located at 1367 cm^{-1}. As compared to that of h-BN powder samples, an 8 cm^{-1} downshift is found in the composites (inset of Figure 2b), suggesting the existence of a strong interaction between the h-BN and Cu_2O. Such interaction leads to a small elongation of B−N bond length, resulting in the shifting of the active E_{2g} mode to lower wavenumbers.[46]

XPS was further employed to investigate the compositions and element chemical states of the samples. Supporting Information Figure S1 shows the XPS survey spectrum of the as-obtained Cu_2O@h-BN composites, specifying the presence of B, N, Cu, O, and C elements in the samples. On the basis of the XPS measurement, the content of h-BN in the composites was roughly determined to be 24 wt %. High-resolution XPS spectra of B 1s and N 1s are shown in Figure 2c. The peak at 190.6 eV in B 1s spectra is assigned to B−N bonds,[51] while a shoulder of 191.6 eV comes from B−O bands formed by B-site

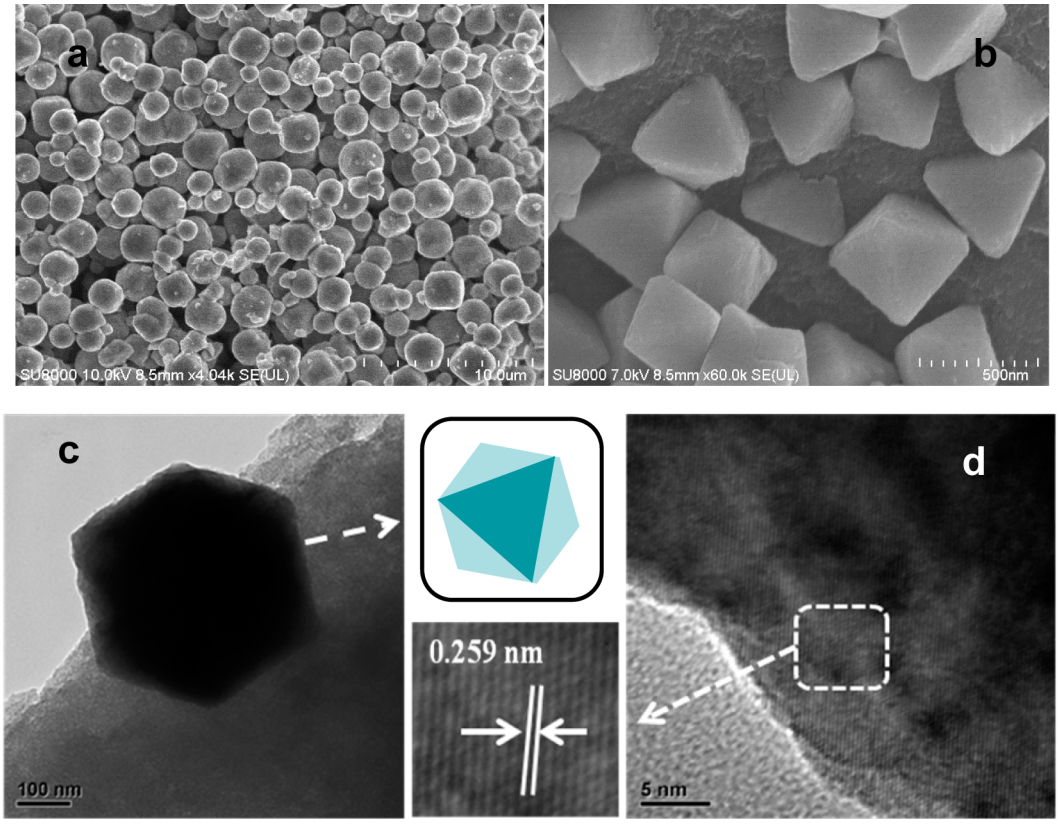

Figure 3. (a) SEM images of Cu_2O, (b) SEM images of Cu_2O@BN composites, (c) TEM images of Cu_2O@BN composites, and (d) the corresponding HRTEM images.

dx.doi.org/10.1021/am5037737 | ACS Appl. Mater. Interfaces 2014, 6, 14469−14476

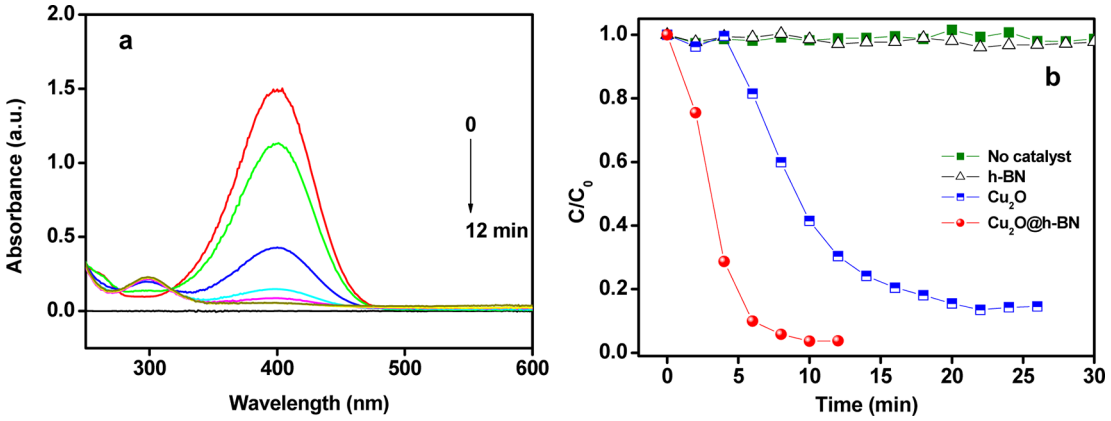

Figure 4. (a) Evolution of UV−vis spectra during *p*-nitrophenol reduction over Cu_2O@h-BN composites. (b) Comparative study of the conversion of *p*-nitrophenol as a function of reaction time with excess amount of $NaBH_4$ over various catalysts: without catalysts, h-BN nanosheets, pure Cu_2O, and Cu_2O@h-BN composites.

hydroxylation,[21] consistent with our above FTIR and Raman analysis. The N 1s core-level XPS spectrum shows a strong photoelectron signal at 398.2 eV, in agreement with literature values for N^{3-} in BN layers.[52,53] As illustrated in Figure 2d, the O 1s spectrum consists of two unresolved peaks located at 530.3 and 531.6 eV. The predominant peak at 530.3 eV corresponds to O^{2-} in the Cu_2O crystal,[54] while the peak at the higher energy of 531.6 eV is attributed to the oxygen species on the surface of Cu_2O.[55,56] The Cu 2p core-level spectrum shows two intense peaks at 932.2 and 952.1 eV, which can be assigned to Cu $2p_{3/2}$ and Cu $2p_{1/2}$ spin−orbital components of Cu(I) specials, respectively,[57] whereas the satellite peaks associated with Cu(II) species are rather weak,[36] suggesting the slight surface oxidation in air under ambient conditions. Therefore, these experimental results demonstrate the successful preparation of chemical-coupling Cu_2O@h-BN composites.

The morphologies and microstructures of the as-prepared Cu_2O and Cu_2O@h-BN composites were examined by SEM and TEM. The representative SEM images of pure Cu_2O without the addition of h-BN suspension are shown in Figure 3a. It can be seen that the pure Cu_2O particles are distributed in the shape of irregular microspheres, which are prone to crumple and agglomerate, resulting in a broad particle size distribution. Encouragingly, after incorporating with h-BN, the Cu_2O particles show regular octahedron morphology, and are well dispersed on the surfaces of h-BN nanosheets (Figure 3b). The size of the Cu_2O nanoparticles dispersed on the h-BN sheets was approximately 300 nm. Actually, the Cu_2O particle size and morphologies are highly dependent on its precursor.[34] Prior to the addition of the reductant glucose, Cu^{2+} ions were reacted with NaOH to form black precursor. When h-BN nanosheets were introduced in the synthesis system, the −OH and −NH groups on the h-BN nanosheets can act as the active sites for anchoring the precursor, which might be beneficial for the formation of regular Cu_2O octahedrons with good dispersion on the h-BN nanosheets after addition of the glucose. Thus, the h-BN is readily expected to be used as a supporter to composite Cu_2O particles on the surfaces. Figure 3c shows the TEM images of Cu_2O@BN composites. The h-BN and Cu_2O components can be easily distinguished due to the differences in contrast. Consistent with the SEM observation, the TEM images show the standing of Cu_2O octahedron on the grid plane of h-BN nanosheets. The lattice fringe of the octahedron-like particle has an interplanar spacing of 0.259 nm (as shown in Figure 3d), which is in agreement with the (111) plane of cubic Cu_2O.[40] Unlike the traditional organic chain-like stabilizers,[7] h-BN nanosheets have two-dimensional structure, which provides a platform for attaching Cu_2O octahedrons and endowing the "naked" particle surface with high active sites, a property that might be beneficial for the catalytic reaction on the surfaces.

The catalytic properties of the samples were evaluated by reduction of *p*-nitrophenol to *p*-aminophenol with $NaBH_4$. Generally, the direct reduction of *p*-nitrophenol over noble metal particles is considered as a green process for the production of *p*-aminophenol.[58−60] Because of their high cost and scarcity of the noble metal, the development of alternative catalysts for the conversion of *p*-nitrophenol to *p*-aminophenol has been actively pursued, including noble-metal-free catalysts,[61] and metal-free materials.[62] Recently, Mandlimath and Gopal found that CuO, Co_3O_4, Fe_2O_3, and NiO could accelerate the conversion of *p*-nitrophenol to *p*-aminophenol, while TiO_2, V_2O_5, Cr_2O_3, MnO_2, and ZnO were inactive toward this conversion.[63] In this study, we reported the first attempt to investigate the feasibility using Cu_2O@h-BN composites as a catalyst for the reduction of *p*-nitrophenol to *p*-aminophenol. Figure 4a shows the time-dependent absorption of solution over Cu_2O@h-BN composites in the presence of excess $NaBH_4$. The maximum absorbance peak at 400 nm gradually declines as the reduction reaction time proceeds, accompanying a concomitant increase of the peak at 300 nm. Moreover, two isosbestic points are observed at 280 and 314 nm, indicating the clean conversion without producing any byproducts.[58] Complete conversion of *p*-nitrophenol to *p*-aminophenol was achieved within 12 min. To specify the role of the Cu_2O@h-BN composites in this conversion, the degree of the conversion is presented by the ratio of the concentration C and the initial value of *p*-nitrophenol C_0, that is, C/C_0, under various conditions. The C/C_0 ratio is obtained by the corresponding absorbance at 400 nm according to the Lambert−Beer law. As shown in Figure 4b, without catalysts, the maximum absorption peak remains unchanged, indicating that $NaBH_4$ alone cannot initiate the conversion reaction even with a large excess amount. Furthermore, the introduction of h-BN into the reaction system also gives a negligible conversion, indicating that h-BN nanosheets are inactive for the reduction of *p*-nitrophenol. After pure Cu_2O was added, the concentration of *p*-nitrophenol was gradually decreased after 5 min

dx.doi.org/10.1021/am5037737 | ACS Appl. Mater. Interfaces 2014, 6, 14469−14476

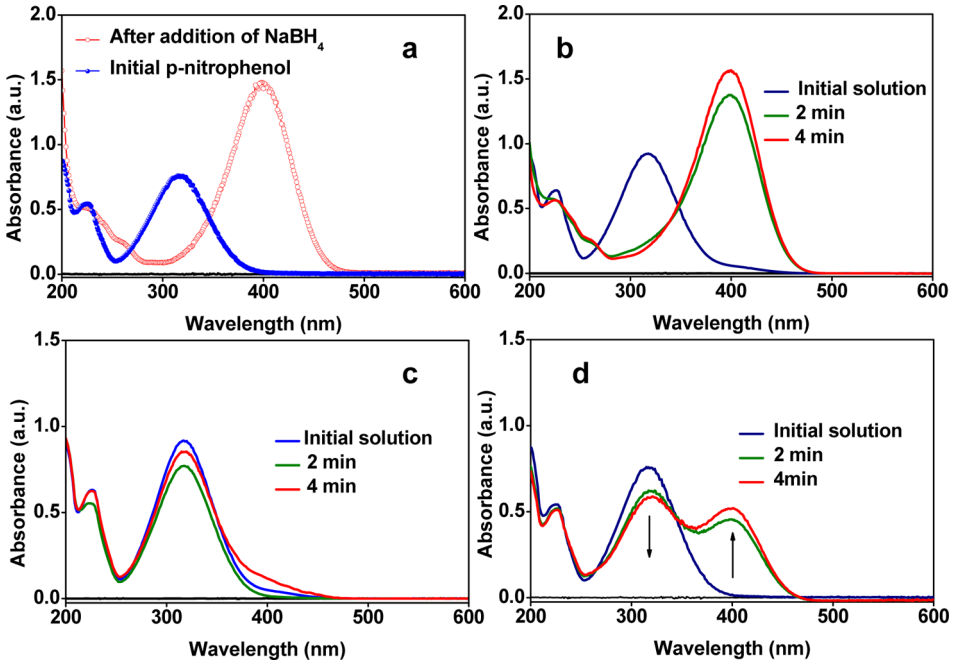

Figure 5. Evolution of UV−vis spectra of the *p*-nitrophenol solution with various additives: (a) adding of $NaBH_4$, (b) adding of h-BN nanosheets, (c) adding of pure Cu_2O, and (d) adding of Cu_2O@h-BN composites.

induction period. Nearly 86% of conversion was achieved after 25 min over Cu_2O samples. Obviously, even though h-BN nanosheets show a negligible activity, the Cu_2O@h-BN composites exhibit the much enhanced catalytic performance for the reduction of *p*-nitrophenol as compared to pure Cu_2O. It should be mentioned that there is no induction period over the Cu_2O@h-BN composites. In general, the induction time is considered to be due to the diffusion for *p*-nitrophenolate ions to be adsorbed onto the catalyst surfaces before the reaction could start.[64−66] Furthermore, it is found that the reduction of *p*-nitrophenol to *p*-aminophenol over Cu_2O@h-BN composites follows the pseudo first-order kinetics (Supporting Information Figure S2).

To gain more insight into this reaction and rationally distinguish the contributors to the conversion reaction, the influence of the $NaBH_4$, h-BN, pure Cu_2O, and Cu_2O@h-BN composites on the evolution of absorption spectra of *p*-nitrophenol were investigated. As illustrated in Figure 5a, the *p*-nitrophenol exhibits a peak at 317 nm in neutral aqueous solution. Upon the addition of $NaBH_4$, the absorption peak was immediately shifted from 317 to 400 nm, because of the formation of *p*-nitrophenolate ions under alkaline condition with $NaBH_4$.[58] However, as discussed above, $NaBH_4$ is not able to reduce the *p*-nitrophenolate ions without catalysts, even though it is considered as the electron donor and hydrogen source. Surprisingly, the spectral shift of the absorption peak was also observed after adding h-BN instead of $NaBH_4$. As shown in Figure 5b, the *p*-nitrophenolate ions become the dominating species in the solution after about 4 min. From the above structural analyses, it is clear that the h-BN possesses a large amount of −OH and −NH groups on the surface. These groups are reasonably regarded as the active sites to adsorb and ionize the *p*-nitrophenolate molecules. Figure 5c shows the time course of UV−vis spectra of *p*-nitrophenol over pure Cu_2O without $NaBH_4$. The intensity of the peak at 317 nm decreases slightly, mainly due to the concentration quenching effect, while the formation of *p*-nitrophenolate ions is rather limited. Apparently, as shown in Figure 5d, Cu_2O@h-BN composites exhibit excellent capability for the ionization of *p*-nitrophenol. That is, despite that the h-BN has no activity for the reduction of *p*-nitrophenol into *p*-aminophenol (Figure 4b), the h-BN component in the composites can act as good adsorbent for the formation of *p*-nitrophenolate ions and keep them at the vicinity of Cu_2O octahedrons. These experimental results can well explain the superior activity of Cu_2O@h-BN composites for the reduction of *p*-nitrophenol with $NaBH_4$. On the basis of these results, the mechanisms of conversion of *p*-nitrophenol over Cu_2O@h-BN composites are speculated in Figure 6. The *p*-nitrophenolate ions are adsorbed by the h-BN

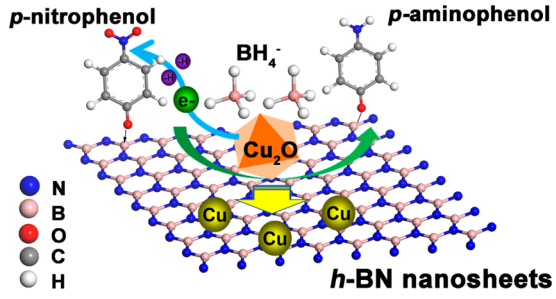

Figure 6. Schematic of the reduction of *p*-nitrophenol to *p*-aminophenol over the Cu_2O@h-BN composites.

component; at the same time, brohydride ions react with the Cu_2O component in the composites and transfer a surface hydrogen species and electrons to them, thereby resulting in the efficient reduction of the $-NO_2$ group of *p*-nitrophenol to the $-NH_2$ group.[58] That is, there exists a beneficial effect of dispersing Cu_2O on h-BN nanosheets and their synergetic effects in the Cu_2O@h-BN composites.

Because the $NaBH_4$ belongs to a strong reducing agent, the cycling catalytic performances of the Cu_2O@h-BN composites in the conversion of *p*-nitrophenol with excess amount of

dx.doi.org/10.1021/am5037737 | ACS Appl. Mater. Interfaces 2014, 6, 14469−14476

$NaBH_4$ are further investigated under the same condition. As shown in Supporting Information Figure S3, the catalytic activity gradually decreases with cycle times. After four cycle tests, the activity was decreased to 50% of the initial efficiency. To further explore this phenomenon, XRD patterns for Cu_2O@h-BN composite before and after cycling reaction have been collected and compared. As displayed in Supporting Information Figure S4, the characteristic peaks of Cu_2O gradually disappear, while the (111) peak of metallic Cu at 43.3° becomes stronger in intensity with the running cycling reaction. That is, the Cu_2O component was gradually reduced to Cu metallic particles by $NaBH_4$. It should be mentioned that it is very difficult to simply compare the activities of Cu_2O and metallic Cu, because the catalytic activity depends on several factors including the particle sizes, morphologies, and surface properties. Encouragingly, even though the Cu_2O component was chemically not stable, the composites still show the evident activity for the *p*-nitrophenol reduction after four cycle tests, because the resulting metallic Cu particles also show the activity for the conversion of *p*-nitrophenol,[67] which has significant importance for the application in the reduction of *p*-nitrophenol to *p*-aminophenol.

CONCLUSION

We have succeeded in developing a conceptually different method to disperse Cu_2O octahedrons on the surfaces of h-BN nanosheets, and initially found that the as-obtained Cu_2O@h-BN composites can be used in the conversion reaction of *p*-nitrophenol to *p*-aminophenol. Furthermore, the detailed structures of the composites were fully characterized by XRD, FTIR, Raman spectra, XPS, SEM, and TEM. It is found that the h-BN component in the composites can act as the active adsorbent for formation and adsorbance of the *p*-nitrophenolate ions, while Cu_2O components react with BH_4^- ions and transfer a surface hydrogen species and electrons, resulting in the reduction of the $-NO_2$ group of *p*-nitrophenol to the $-NH_2$ group. Our results suggest that the h-BN nanosheets can be expected to be a good supporter to incorporate the functional metal oxides, which open the way to a range of important applications of h-BN-based materials.

ASSOCIATED CONTENT

Supporting Information

Survey XPS, cycling catalytic performances for the reduction of *p*-nitrophenol, and XRD patterns of the Cu_2O@h-BN composites before and after the conversion reaction. This material is available free of charge via the Internet at http://pubs.acs.org.

AUTHOR INFORMATION

Corresponding Author

*E-mail: qiuxq@fzu.edu.cn.

Author Contributions

C.H. and W.Y. carried out the synthesis, characterization, and manuscript writing. Q.L. performed reactivity studies of the samples. X.Q. designed and directed the project and manuscript writing. All authors have given approval to the final version of the manuscript.

Notes

The authors declare no competing financial interest.

ACKNOWLEDGMENTS

This project was sponsored by the Scientific Research Foundation for the Returned Overseas Chinese Scholars, State Education Ministry. This work was also financially supported by National Basic Research Program of China (973 Program) (2013CB632405), the National Natural Science Foundation of China (NSFC, Grant nos. 21273038 and U1033603), and the Fund of Key Laboratory of Optoelectronic Materials Chemistry and Physics, Chinese Academy of Sciences (2008DP173016).

REFERENCES

(1) Fernandez-Garcia, M.; Martinez-Arias, A.; Hanson, J.; Rodriguez, J. Nanostructured Oxides in Chemistry: Characterization and Properties. *Chem. Rev.* **2004**, *104*, 4063−4104.

(2) Kolmakov, A.; Moskovits, M. Chemical Sensing and Catalysis by One-Dimensional Metal-Oxide Nanostructures. *Annu. Rev. Mater. Res.* **2004**, *34*, 151−180.

(3) Wang, X.; Zhuang, J.; Peng, Q.; Li, Y. A General Strategy for Nanocrystal Synthesis. *Nature* **2005**, *437*, 121−124.

(4) Keller, A. A.; Wang, H.; Zhou, D.; Lenihan, H. S.; Cherr, G.; Cardinale, B. J.; Miller, R.; Ji, Z. Stability and Aggregation of Metal Oxide Nanoparticles in Natural Aqueous Matrices. *Environ. Sci. Technol.* **2010**, *44*, 1962−1967.

(5) Fei, H.; Peng, Z.; Li, L.; Yang, Y.; Lu, W.; Samuel, E. L.; Fan, X.; Tour, J. M. Preparation of Carbon-Coated Iron Oxide Nanoparticles Dispersed on Graphene Sheets and Applications as Advanced Anode Materials for Lithium-Ion Batteries. *Nano Res.* **2014**, *7*, 1−9.

(6) Reddy, A. L. M.; Ramaprabhu, S. Nanocrystalline Metal Oxides Dispersed Multiwalled Carbon Nanotubes as Supercapacitor Electrodes. *J. Phys. Chem. C* **2007**, *111*, 7727−7734.

(7) Sarkar, S.; Guibal, E.; Quignard, F.; SenGupta, A. Polymer-Supported Metals and Metal Oxide Nanoparticles: Synthesis, Characterization, and Applications. *J. Nanopart. Res.* **2012**, *14*, 1−24.

(8) Wang, D.; Choi, D.; Li, J.; Yang, Z.; Nie, Z.; Kou, R.; Hu, D.; Wang, C.; Saraf, L. V.; Zhang, J. Self-Assembled TiO_2−Graphene Hybrid Nanostructures for Enhanced Li-Ion Insertion. *ACS Nano* **2009**, *3*, 907−914.

(9) Wang, G.; Tan, X.; Zhou, Q.; Liu, Y.; Wang, M.; Yang, L. Synthesis of Highly Dispersed Zinc Oxide Nanoparticles on Carboxylic Graphene for Development a Sensitive Acetylcholinesterase Biosensor. *Sens. Actuators, B* **2014**, *190*, 730−736.

(10) Zhou, W.; Zhu, J.; Cheng, C.; Liu, J.; Yang, H.; Cong, C.; Guan, C.; Jia, X.; Fan, H. J.; Yan, Q. A General Strategy toward Graphene@Metal Oxide Core−Shell Nanostructures for High-Performance Lithium Storage. *Energy Environ. Sci.* **2011**, *4*, 4954−4961.

(11) Li, W.; Wang, F.; Feng, S.; Wang, J.; Sun, Z.; Li, B.; Li, Y.; Yang, J.; Elzatahry, A. A.; Xia, Y. Sol−Gel Design Strategy for Ultradispersed TiO_2 Nanoparticles on Graphene for High-Performance Lithium Ion Batteries. *J. Am. Chem. Soc.* **2013**, *135*, 18300−18303.

(12) Xu, C.; Wang, X. Graphene Oxide-Mediated Synthesis of Stable Metal Nanoparticle Colloids. *Colloids Surf., A* **2012**, *404*, 78−82.

(13) Dean, C.; Young, A.; Meric, I.; Lee, C.; Wang, L.; Sorgenfrei, S.; Watanabe, K.; Taniguchi, T.; Kim, P.; Shepard, K. Boron Nitride Substrates for High-Quality Graphene Electronics. *Nat. Nanotechnol.* **2010**, *5*, 722−726.

(14) Song, L.; Ci, L.; Lu, H.; Sorokin, P. B.; Jin, C.; Ni, J.; Kvashnin, A. G.; Kvashnin, D. G.; Lou, J.; Yakobson, B. I. Large Scale Growth and Characterization of Atomic Hexagonal Boron Nitride Layers. *Nano Lett.* **2010**, *10*, 3209−3215.

(15) Liu, Z.; Gong, Y.; Zhou, W.; Ma, L.; Yu, J.; Idrobo, J. C.; Jung, J.; MacDonald, A. H.; Vajtai, R.; Lou, J. Ultrathin High-Temperature Oxidation-Resistant Coatings of Hexagonal Boron Nitride. *Nat. Commun.* **2013**, *4*, 2541.

(16) Lei, W.; Portehault, D.; Liu, D.; Qin, S.; Chen, Y. Porous Boron Nitride Nanosheets for Effective Water Cleaning. *Nat. Commun.* **2013**, *4*, 1777.

(17) Chen, W.; Li, Y.; Yu, G.; Li, C.-Z.; Zhang, S. B.; Zhou, Z.; Chen, Z. Hydrogenation: A Simple Approach to Realize Semiconductor−Half-Metal−Metal Transition in Boron Nitride Nanoribbons. *J. Am. Chem. Soc.* **2010**, *132*, 1699−1705.
(18) Haubner, R.; Wilhelm, M.; Weissenbacher, R.; Lux, B. Boron Nitrides−Properties, Synthesis and Applications. In *High Performance Non-Oxide Ceramics II*; Jansen, M., Ed.; Springer: Berlin Heidelberg, 2002.
(19) Watanabe, K.; Taniguchi, T.; Kanda, H. Direct-Bandgap Properties and Evidence for Ultraviolet Lasing of Hexagonal Boron Nitride Single Crystal. *Nat. Mater.* **2004**, *3*, 404−409.
(20) Watanabe, K.; Taniguchi, T.; Niiyama, T.; Miya, K.; Taniguchi, M. Far-Ultraviolet Plane-Emission Handheld Device Based on Hexagonal Boron Nitride. *Nat. Photonics* **2009**, *3*, 591−594.
(21) Lei, W.; Portehault, D.; Dimova, R.; Antonietti, M. Boron Carbon Nitride Nanostructures from Salt Melts: Tunable Water-Soluble Phosphors. *J. Am. Chem. Soc.* **2011**, *133*, 7121−7127.
(22) Li, L. H.; Chen, Y.; Cheng, B.-M.; Lin, M. Y.; Chou, S. L.; Peng, Y. C. Photoluminescence of Boron Nitride Nanosheets Exfoliated by Ball Milling. *Appl. Phys. Lett.* **2012**, *100*, 261108.
(23) Stankovich, S.; Dikin, D. A.; Dommett, G. H.; Kohlhaas, K. M.; Zimney, E. J.; Stach, E. A.; Piner, R. D.; Nguyen, S. T.; Ruoff, R. S. Graphene-Based Composite Materials. *Nature* **2006**, *442*, 282−286.
(24) Li, N.; Xiao, Y.; Hu, C.; Cao, M. Microwave-Assisted Synthesis of Dual-Conducting Cu_2O@Cu-Graphene System with Improved Electrochemical Performance as Anode Material for Lithium Batteries. *Chem.—Asian J.* **2013**, *8*, 1960−1965.
(25) Wang, P.; Wang, J.; Ming, T.; Wang, X.; Yu, H.; Yu, J.; Wang, Y.; Lei, M. Dye-Sensitization-Induced Visible-Light Reduction of Graphene Oxide for the Enhanced TiO_2 Photocatalytic Performance. *ACS Appl. Mater. Interfaces* **2013**, *5*, 2924−2929.
(26) Lin, Y.; Connell, J. W. Advances in 2D Boron Nitride Nanostructures: Nanosheets, Nanoribbons, Nanomeshes, and Hybrids with Graphene. *Nanoscale* **2012**, *4*, 6908−6939.
(27) Lin, Y.; Williams, T. V.; Xu, T. B.; Cao, W.; Elsayed-Ali, H. E.; Connell, J. W. Aqueous Dispersions of Few-Layered and Monolayered Hexagonal Boron Nitride Nanosheets from Sonication-Assisted Hydrolysis: Critical Role of Water. *J. Phys. Chem. C* **2011**, *115*, 2679−2685.
(28) Zheng, M.; Liu, Y.; Gu, Y.; Xu, Z. Synthesis and Characterization of Boron Nitride Sponges as a Novel Support for Metal Nanoparticles. *Sci. China, Ser. B: Chem.* **2008**, *51*, 205−210.
(29) Wu, J.; Chen, W.-C. A Novel Bn Supported Bi-Metal Catalyst for Selective Hydrogenation of Crotonaldehyde. *Appl. Catal., A* **2005**, *289*, 179−185.
(30) Hara, M.; Kondo, T.; Komoda, M.; Ikeda, S.; N. Kondo, J.; Domen, K.; Hara, M.; Shinohara, K.; Tanaka, A. Cu_2O as a Photocatalyst for Overall Water Splitting under Visible Light Irradiation. *Chem. Commun.* **1998**, 357−358.
(31) Pang, H.; Gao, F.; Lu, Q. Morphology Effect on Antibacterial Activity of Cuprous Oxide. *Chem. Commun.* **2009**, 1076−1078.
(32) Kevin, M.; Ong, W.; Lee, G.; Ho, G. Formation of Hybrid Structures: Copper Oxide Nanocrystals Templated on Ultralong Copper Nanowires for Open Network Sensing at Room Temperature. *Nanotechnology* **2011**, *22*, 235701.
(33) Rai, B. Cu_2O Solar Cells: A Review. *Sol. Cells* **1988**, *25*, 265−272.
(34) Huang, C.; Zheng, L.; Miyauchi, M.; Qiu, X. A Facile One-Pot Synthesis of Cu-Cu_2O Concave Cube Hybrid Architectures. *CrystEngComm* **2014**, *16*, 4967−4972.
(35) Poizot, P.; Laruelle, S.; Grugeon, S.; Dupont, L.; Tarascon, J. Nano-Sized Transition-Metal Oxides as Negative-Electrode Materials for Lithium-Ion Batteries. *Nature* **2000**, *407*, 496−499.
(36) Qiu, X.; Miyauchi, M.; Sunada, K.; Minoshima, M.; Liu, M.; Lu, Y.; Li, D.; Shimodaira, Y.; Hosogi, Y.; Kuroda, Y. Hybrid Cu_xO/TiO_2 Nanocomposites as Risk-Reduction Materials in Indoor Environments. *ACS Nano* **2012**, *6*, 1609−1618.
(37) Tran, P. D.; Batabyal, S. K.; Pramana, S. S.; Barber, J.; Wong, L. H.; Loo, S. C. J. A Cuprous Oxide−Reduced Graphene Oxide (Cu_2O-rGO) Composite Photocatalyst for Hydrogen Generation: Employing rGo as an Electron Acceptor to Enhance the Photocatalytic Activity and Stability of Cu_2O. *Nanoscale* **2012**, *4*, 3875−3878.
(38) Zhigang, N. Reduced Graphene Oxide-Cuprous Oxide Hybrid Nanopowders: Hydrothermal Synthesis and Enhanced Photocatalytic Performance under Visible Light Irradiation. *Mater. Sci. Semicond. Process.* **2014**, *23*, 78−84.
(39) Gao, Z.; Liu, J.; Xu, F.; Wu, D.; Wu, Z.; Jiang, K. One-Pot Synthesis of Graphene−Cuprous Oxide Composite with Enhanced Photocatalytic Activity. *Solid State Sci.* **2012**, *14*, 276−280.
(40) Yan, X. Y.; Tong, X. L.; Zhang, Y. F.; Han, X. D.; Wang, Y. Y.; Jin, G. Q.; Qin, Y.; Guo, X. Y. Cuprous Oxide Nanoparticles Dispersed on Reduced Graphene Oxide as an Efficient Electrocatalyst for Oxygen Reduction Reaction. *Chem. Commun.* **2012**, *48*, 1892−1894.
(41) Huang, C.; Chen, C.; Ye, X.; Ye, W.; Hu, J.; Xu, C.; Qiu, X. Stable Colloidal Boron Nitride Nanosheet Dispersion and Its Potential Application in Catalysis. *J. Mater. Chem. A* **2013**, *1*, 12192−12197.
(42) Soltani, A.; Bakhtiar, H.; Thevenin, P.; Bath, A. Optical Properties of Thin Hexagonal Boron Nitride Layers. *J. Fiz. UTM* **2003**, *9*, 21−29.
(43) Paine, R. T.; Narula, C. K. Synthetic Routes to Boron Nitride. *Chem. Rev.* **1990**, *90*, 73−91.
(44) Kuo, C. H.; Huang, M. H. Facile Synthesis of Cu_2O Nanocrystals with Systematic Shape Evolution from Cubic to Octahedral Structures. *J. Phys. Chem. C* **2008**, *112*, 18355−18360.
(45) Borgohain, K.; Murase, N.; Mahamuni, S. Synthesis and Properties of Cu_2O Quantum Particles. *J. Appl. Phys.* **2002**, *92*, 1292−1297.
(46) Arenal, R.; Ferrari, A.; Reich, S.; Wirtz, L.; Mevellec, J. Y.; Lefrant, S.; Rubio, A.; Loiseau, A. Raman Spectroscopy of Single-Wall Boron Nitride Nanotubes. *Nano Lett.* **2006**, *6*, 1812−1816.
(47) Nemanich, R.; Solin, S.; Martin, R. M. Light Scattering Study of Boron Nitride Microcrystals. *Phys. Rev. B* **1981**, *23*, 6348.
(48) Compaan, A.; Cummins, H. Resonant Quadrupole-Dipole Raman Scattering at the 1s Yellow Exciton in Cu_2O. *Phys. Rev. Lett.* **1973**, *31*, 41−44.
(49) Mao, Y.; He, J.; Sun, X.; Li, W.; Lu, X.; Gan, J.; Liu, Z.; Gong, L.; Chen, J.; Liu, P. Electrochemical Synthesis of Hierarchical Cu_2O Stars with Enhanced Photoelectrochemical Properties. *Electrochim. Acta* **2012**, *62*, 1−7.
(50) Yu, P. Y.; Shen, Y. Resonance Raman Studies in Cu_2O. Ii. The Yellow and Green Excitonic Series. *Phys. Rev. B* **1978**, *17*, 4017−4030.
(51) Ci, L.; Song, L.; Jin, C.; Jariwala, D.; Wu, D.; Li, Y.; Srivastava, A.; Wang, Z.; Storr, K.; Balicas, L. Atomic Layers of Hybridized Boron Nitride and Graphene Domains. *Nat. Mater.* **2010**, *9*, 430−435.
(52) Nazarov, A. S.; Demin, V. N.; Grayfer, E. D.; Bulavchenko, A. I.; Arymbaeva, A. T.; Shin, H. J.; Choi, J. Y.; Fedorov, V. E. Functionalization and Dispersion of Hexagonal Boron Nitride (h-BN) Nanosheets Treated with Inorganic Reagents. *Chem.—Asian J.* **2012**, *7*, 554.
(53) Shi, Y.; Hamsen, C.; Jia, X.; Kim, K. K.; Reina, A.; Hofmann, M.; Hsu, A. L.; Zhang, K.; Li, H.; Juang, Z. Y. Synthesis of Few-Layer Hexagonal Boron Nitride Thin Film by Chemical Vapor Deposition. *Nano Lett.* **2010**, *10*, 4134−4139.
(54) Li, B.; Cao, H.; Yin, G.; Lu, Y.; Yin, J. Cu_2O@Reduced Graphene Oxide Composite for Removal of Contaminants from Water and Supercapacitors. *J. Mater. Chem.* **2011**, *21*, 10645−10648.
(55) Wang, W. Z.; Wang, G.; Wang, X. S.; Zhan, Y.; Liu, Y.; Zheng, C. L. Synthesis and Characterization of Cu_2O Nanowires by a Novel Reduction Route. *Adv. Mater.* **2002**, *14*, 67−69.
(56) Yao, K. X.; Yin, X. M.; Wang, T. H.; Zeng, H. C. Synthesis, Self-Assembly, Disassembly, and Reassembly of Two Types of Cu_2O Nanocrystals Unifaceted with {001} or {110} Planes. *J. Am. Chem. Soc.* **2010**, *132*, 6131−6144.
(57) Qiu, X.; Liu, M.; Sunada, K.; Miyauchi, M.; Hashimoto, K. A Facile One-Step Hydrothermal Synthesis of Rhombohedral $CuFeO_2$ Crystals with Antivirus Property. *Chem. Commun.* **2012**, *48*, 7365−7367.

(58) Herves, P.; Pérez-Lorenzo, M.; Liz-Marzán, L. M.; Dzubiella, J.; Lu, Y.; Ballauff, M. Catalysis by Metallic Nanoparticles in Aqueous Solution: Model Reactions. *Chem. Soc. Rev.* **2012**, *41*, 5577−5587.
(59) Pozun, Z. D.; Rodenbusch, S. E.; Keller, E.; Tran, K.; Tang, W.; Stevenson, K. J.; Henkelman, G. A Systematic Investigation of p-Nitrophenol Reduction by Bimetallic Dendrimer Encapsulated Nanoparticles. *J. Phys. Chem. C* **2013**, *117*, 7598−7604.
(60) Hayakawa, K.; Yoshimura, T.; Esumi, K. Preparation of Gold-Dendrimer Nanocomposites by Laser Irradiation and Their Catalytic Reduction of 4-Nitrophenol. *Langmuir* **2003**, *19*, 5517−5521.
(61) Su, Y.; Lang, J.; Li, L.; Guan, K.; Du, C.; Peng, L.; Han, D.; Wang, X. Unexpected Catalytic Performance in Silent Tantalum Oxide through Nitridation and Defect Chemistry. *J. Am. Chem. Soc.* **2013**, *135*, 11433−11436.
(62) Kong, X. K.; Sun, Z. Y.; Chen, M.; Chen, Q. W. Metal-Free Catalytic Reduction of 4-Nitrophenol to 4-Aminophenol by N-Doped Graphene. *Energy Environ. Sci.* **2013**, *6*, 3260−3266.
(63) Mandlimath, T. R.; Gopal, B. Catalytic Activity of First Row Transition Metal Oxides in the Conversion of p-Nitrophenol to p-Aminophenol. *J. Mol. Catal. A: Chem.* **2011**, *350*, 9−15.
(64) Wunder, S.; Polzer, F.; Lu, Y.; Mei, Y.; Ballauff, M. Kinetic Analysis of Catalytic Reduction of 4-Nitrophenol by Metallic Nanoparticles Immobilized in Spherical Polyelectrolyte Brushes. *J. Phys. Chem. C* **2010**, *114*, 8814−8820.
(65) Zeng, J.; Zhang, Q.; Chen, J.; Xia, Y. A Comparison Study of the Catalytic Properties of Au-Based Nanocages, Nanoboxes, and Nanoparticles. *Nano Lett.* **2009**, *10*, 30−35.
(66) Han, L.; Zhu, C.; Wang, L.; Dong, S. Facile Synthesis of Chain-Like Cocu Bimetallic Nanomaterials and Their Catalytic Properties. *Catal. Sci. Technol.* **2013**, *3*, 1501−1504.
(67) Zhang, P.; Sui, Y.; Xiao, G.; Wang, Y.; Wang, C.; Liu, B.; Zou, G.; Zou, B. Facile Fabrication of Faceted Copper Nanocrystals with High Catalytic Activity for p-Nitrophenol Reduction. *J. Mater. Chem. A* **2013**, *1*, 1632−1638.